

Automatic Reconstruction of 3D Geometry Using Projections and a Geometric Prior Model

J. Lötjönen^{1,2,3}, I. E. Magnin², L. Reinhardt^{1,3}, J. Nenonen^{1,3}, and T. Katila^{1,3}

¹ Laboratory of Biomedical Engineering

Helsinki University of Technology, P.O.B. 2200, FIN-02015 HUT, Finland
{Jyrki.Lotjonen,Lutz.Reinhardt,Jukka.Nenonen,Toivo.Katila}@hut.fi

² Creatis, INSA 502, 69621 Villeurbanne Cedex, France

Isabelle.Magnin@creatis.insa-lyon.fr

³ BioMag Laboratory

Helsinki University Central Hospital, P.O.B. 503, FIN-00029 HYKS, Finland

Abstract. A method has been developed to reconstruct 3D surfaces from two orthogonal X-ray projections. A 3D geometrical prior model, composed of triangulated surfaces, is deformed according to contours segmented from projection images. The contours are segmented by a new method based on free-form deformation. First, virtual X-ray images of the prior model are constructed by simulating real X-ray imaging. Thereafter, the contours segmented from the virtual projections are elastically matched with patient data. Next, the produced 2D vectors are back-projected onto the surface of the prior model and the prior model is deformed using the back-projected vectors with shape-based interpolation. The accuracy of the method is validated by a data set containing 20 cases. The method is applied to reconstruct thorax and lung surfaces. The average matching error is about 1.2 voxels, corresponding to 5 mm.

1 Introduction

Modern medical imaging devices produce detailed 3D volume images. However, these imaging modalities are not always available. Hence, a method to reconstruct individualized 3D information using only two approximately orthogonal X-ray projections was developed. In this paper, the method is demonstrated with two applications: creation of patient specific thorax models and reconstruction of lung volumes from the X-ray projections. Patient-specific thorax models are needed in magnetocardiographic (MCG) and electrocardiographic (ECG) forward and inverse problems [1].

Terzopoulos *et al.* [2] presented a method to recover the 3D shape from 2D profiles of an object using a deformable tube coupled to a deformable spine. The deformation was controlled by physically based intrinsic and extrinsic forces. Bardinet *et al.* [3] proposed a method to match a parametric deformable model to unstructured 3D data. First, they matched a superquadric model to a given point set. Second, the generated superquadric model was deformed locally by a free-form deformation (FFD) [4] using a 3D deformation grid. Because of the parametric model and the regularization, the method can be used to model

sparse data. Several other methods exist to create a 3D surface from a set of 3D points [5,6]. However, the application of these methods to projection images has not been reported. Laurentini has discussed theoretical limitations of surface reconstruction from 2D silhouettes [7].

Our method differs considerably from the methods referred above. In general, the detailed 3D reconstruction of the geometry is not possible using only information from two orthogonal projections. We introduce a method based on 3D elastic deformation of a geometric prior model. First, the contours, created from the prior model by simulating real X-ray imaging conditions, are elastically matched with the contours extracted from real projections. The segmentation method proposed in this paper produces elastic matching between the contours automatically. Second, the generated 2D-vector field is back-projected onto the 3D surface of the model. Finally, the deformation of the prior model is accomplished by shape-based interpolation utilizing the back-projected 3D vectors.

2 Segmentation

The segmentation is based on our previous work [8]. The most important difference is the definition of the prior model. Compared to magnetic resonance (MR) images, edges are smoother and more difficult to define in X-ray projections. Therefore, distance maps, calculated from binarized edges in MR data and used to attract the prior model surfaces in 3D or contours in 2D, can not be easily utilized with X-ray images. In this paper, the prior model is an X-ray image similar to the one to be segmented but taken from a different patient (Fig. 1). The prior model is a representative of mean anatomy. The model is matched with the input image using the FFD in such a way that the similarity between two images is maximized. Since the model is pre-segmented, the segmentation of the input image is automatically produced. Therefore, even very weak edges can be correctly localized because they appear in same positions both in the input image and in the prior model. In practice, we matched the gradient images calculated by the Canny-operator (Fig. 1) [9] because they are less sensitive to the contrast and brightness differences than the original X-ray images. The matching error E_{data} between the model and data is defined by

$$E_{data} = \frac{1}{N_G} \sum_{i=1}^{N_G} \|\mathbf{G}^D(x_i, y_i) - \mathbf{G}_i^M\|^2, \quad (1)$$

where the function $\mathbf{G}^D(x, y)$ is the gradient image of input data, \mathbf{G}_i^M is a gradient vector from the gradient image of the prior model, and N_G is the total number of these vectors. The function $\mathbf{G}^D(x, y)$ is evaluated at the position (x_i, y_i) of the gradient \mathbf{G}_i^M . The symbol $\|\ \|$ denotes vector norm. It is worth noting that the function $\mathbf{G}^D(x, y)$ and the gradients \mathbf{G}_i^M remain constant during deformation. Only the position (x_i, y_i) of each model gradient is varying.

The minimization of E_{data} does not guarantee that the prior knowledge of the model shape is preserved. Therefore, deformation is regularized. The changes in

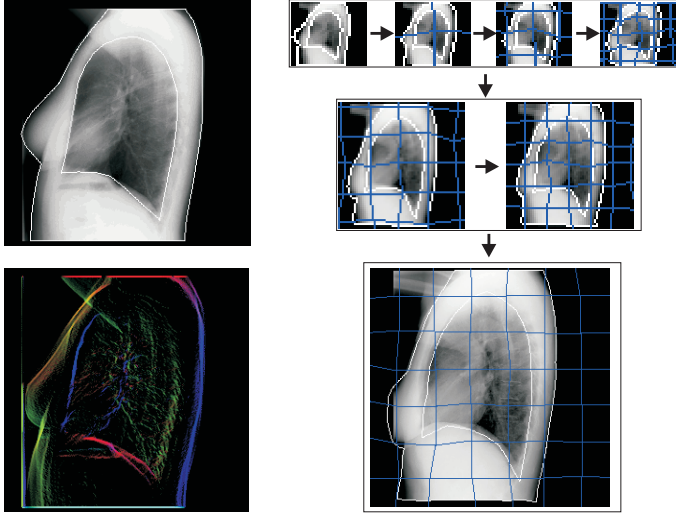


Fig. 1. *On the left: The prior model (up) and corresponding gradient image (bottom), showing only the magnitude of the gradient. On the right: the multi-resolution and the global-to-local approach. The deformed prior model contour and a deformation grid are superimposed onto the input data.*

the normal directions of the contour points, defined by the pre-segmented model, are restricted. The energy E_{model} is calculated as follows

$$E_{model} = \frac{1}{N_C} \sum_{l=1}^{N_C} (1.0 - \mathbf{n}_l \cdot \mathbf{n}_l^*), \quad (2)$$

where N_C is the total number of contour points in the model, \mathbf{n}_l and \mathbf{n}_l^* are the deformed and the original normals of the contour point l , respectively, and \cdot stands for the dot product. Other regularization terms, such as curvature based measures, could be also used [8].

The total energy E_{total} is defined by

$$E_{total} = E_{data} + \gamma E_{model}, \quad (3)$$

where γ is a parameter to control the balance between the two energy components.

The FFD is controlled by a deformation grid. The relation between the displacements of the grid points and the points of the prior model were defined by bilinear interpolation.

Since distance maps are not used, the minimization process is more sensitive to local minima. Two different methods were chosen to improve robustness:

1. The multiresolution approach is used, i.e. the matching is started at a low resolution level and followed by increasing resolution during the process. The

method is a trade off between computation time and convergence towards the global minimum. The multiresolution approach is visualized by vertical arrows in Fig. 1.

2. The *global-to-local* approach is used, i.e. more degrees of freedom are added to the model during deformation. First, input data and the prior model are coarsely registered. In this paper, this is accomplished by matching the centers of mass when the mass of each pixel is the magnitude of the gradient (the first image on the right side of Fig.1). Next, the prior model is deformed by a grid size of 3×3 . When a minimum is found, the number of grid points is increased. In practice, only one grid point is added in both directions at each step until the specified grid size is reached. The highest grid size used depends on the geometric details needed. A grid size of 10×10 is usually large enough for thorax images. After reaching the highest grid size the resolution level is changed. The global-to-local approach is demonstrated by horizontal arrows in Fig. 1.

Local rigidity constraints can be easily added to the prior model. One coefficient can be attached to each prior model vector in Eq. 1. Similar effects with lower computation time can be achieved by locally reducing the number of prior model gradients (Eq. 1). Local rigidity is increased at areas where the model does not represent data well. Moreover, rigidity can be set higher at areas where the gradients are nearly constant in order to reduce computation time.

3 Reconstruction of the 3D Geometry

3.1 Prior Model

The prior model should be a good representation of the object to be modeled. Cootes *et al.* [10] and Székely *et al.* [11] propose 3D models which represent mean shapes in a statistical sense. Moreover, the models are deformed using deformation modes, which are statistically defined using a training set. In our approach, a prior model library was constructed from MR data of ten different subjects. The geometric prior models (Fig. 2a) were built by triangulating the segmented MR volumes [12].

The matching between real data and the prior model can not be accomplished straightforwardly, because the X-ray projections are in 2D and the model in 3D. Therefore, virtual projections are produced from the model by simulating X-ray imaging conditions, i.e. the orthogonal side and frontal views are generated. The distances from the film to the X-ray source and to a patient correspond to the values used in clinical practice. The X-ray source is regarded as a point because the blurring effect is less than one millimeter. Noise is added to the signal. The imaging process has been simplified in two ways: 1) The radiation is monochromatic, 2) The bone structures were excluded because CT images covering the whole thorax were not available for this study. Despite these simplifications, the virtual X-ray images correspond visually well to real images (Fig. 2b). Since the surfaces of the body and lungs are to be reconstructed, the effect of the excluded ribs is not important.

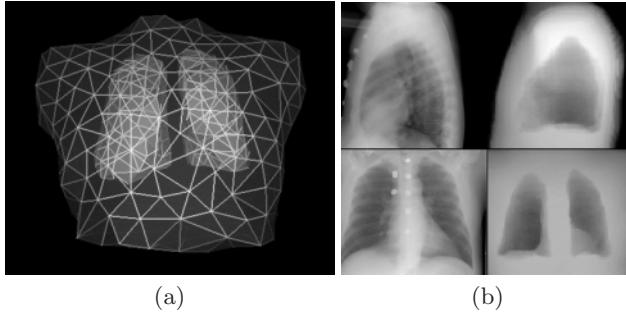


Fig. 2. *a) The prior model. b) Real (left) and virtual (right) X-ray projections.*

3.2 Sparse Vector Field

The contours extracted from real and virtual X-ray projections are matched elastically. The segmentation method automatically gives a 2D displacement vector \mathbf{V}_k for each contour point of the virtual X-ray image (Fig. 3a).

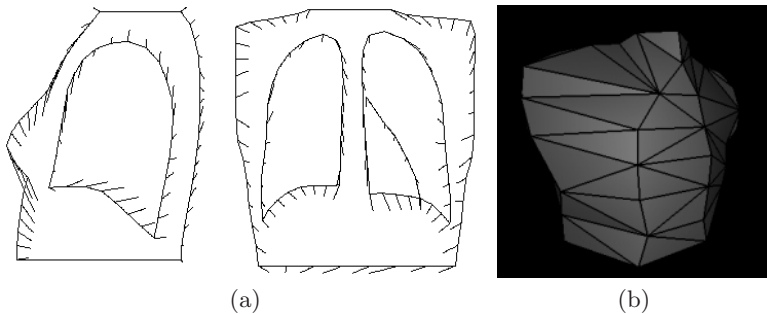


Fig. 3. *a) Displacement vectors of the contour points produced by segmentation. b) The positions of the back-projected contour points on the surface of the 3D prior model.*

Thereafter, each vector is back-projected onto the surface of the 3D prior model. A ray is cast from each contour point towards the X-ray source. The closest surface points, to which the ray is tangential, are selected and denoted by \mathbf{p}_k . Because of parallax effect, the symmetry of the thorax has to be taken into account separately. Next, the vector \mathbf{V}_k is back-projected onto the plane, which is orthogonal to the ray going through the point \mathbf{p}_k and which contains the point \mathbf{p}_k . The end-points of the vector \mathbf{V}_k are projected separately. The projection is accomplished by the ray from the point to be projected to the X-ray source. The effect of parallax effect to the length of the projected vector is automatically considered. Back-projection leads to a sparse 3D vector field. In Fig. 3b, the apex points of the triangles represent the positions \mathbf{p}_k .

3.3 Dense Vector Field

To deform the prior model, the displacement vectors have to be defined for each node of the model \mathbf{p}_l^* (Fig. 2a). Each displacement vector \mathbf{v}_l^* is a weighted sum of the back-projected vectors \mathbf{v}_k . Only the vectors \mathbf{v}_k located close to the node \mathbf{p}_l^* affect the vector \mathbf{v}_l^* . We consider a geodesic distance between the points, computed on the model surface. This is similar to the so-called natural neighbor coordinate used in the computational geometry and geological modeling. The geodesic closeness is defined using the Voronoi areas on the surface for the all points \mathbf{p}_k and each prior model node \mathbf{p}_l^* separately [12]. The weights s_k for each vector \mathbf{v}_k are calculated as follows:

$$s_k = \frac{1/d_k}{\sum_{m=1}^{N_{nb}} 1/d_m}, \quad (4)$$

where d_k is the geodesic distance from \mathbf{p}_k to \mathbf{p}_l^* on the model surface, and N_{nb} is the number of neighboring Voronoi areas. For non-neighboring Voronoi areas weights s_k are zero. The benefit in using geodesic distances is that in some geometries the model nodes may be close to each others according to Euclidean measures, although they are on different sides of the surface.

Linear interpolation gives optimal results if the surface between the back-projected vectors is well represented by a plane. However, this approximation is not valid for some large triangles in Fig. 3b. Therefore, a heuristic interpolation method was developed tending to preserve the normal direction of the prior model surface. A 2D example of shape based interpolation is shown in Fig. 4a. The thick black line describes the known model surface; \mathbf{v}_k and \mathbf{v}_{k+1} are back-projected vectors. A displacement vector on the dashed line is defined as follows. 1) Search a point \mathbf{p}_l^S in such a way that the angle between the lines, defined by points \mathbf{p}_l^S and \mathbf{p}_k , and \mathbf{p}_l^S and \mathbf{p}_{k+1} , is $\pi/2$. 2) These lines are moved according to the displacement vectors \mathbf{v}_k and \mathbf{v}_{k+1} . The cross-section point of the displaced lines is calculated resulting in the vector \mathbf{v}_l^S . 3) The displacement vector for the point \mathbf{p}_l^L is calculated by linear interpolation between the vectors \mathbf{v}_k and \mathbf{v}_{k+1} . 4) The displacement vector between the points \mathbf{p}_l^S and \mathbf{p}_l^L is defined by linear interpolation with the corresponding vectors, otherwise the vector \mathbf{v}_l^S is used.

In general, the prior shape can not be preserved in 3D but an approximation is used (Fig. 4b). The lines in 2D correspond to planes in 3D. The definition of the planes to define the vector \mathbf{v}_l^S can not be directly transformed to 3D. Instead, the orientation of the plane is defined in 3D by the following two vectors: 1) the vector from the point $\mathbf{p}_k + \mathbf{v}_k$ to the point $\mathbf{p}_{k+1} + \mathbf{v}_{k+1}$ and 2) the vector from the point $(\mathbf{p}_k + \mathbf{p}_{k+1})/2$ to the point \mathbf{p}_l^S .

4 Results

4.1 Segmentation

Segmented thorax X-ray images are shown in Fig. 5. The γ factor was 1000 and the lowest resolution 32×32 . Overall, the results are visually good. Usu-

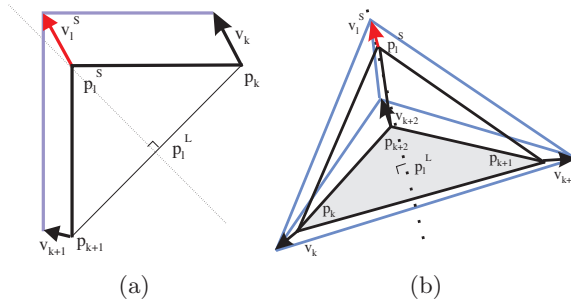


Fig. 4. Shape-based interpolation in 2D and in 3D.



Fig. 5. A segmentation result of thorax images.

ally, only small interactive corrections are needed. The computation time was about 10 seconds using a Sun Ultra10 workstation.

4.2 Extraction of 3D Surfaces

The accuracy of the reconstruction method was tested by a simulation. Virtual X-ray projections were created from 20 segmented MR volumes. The resulting X-ray images were segmented and the prior model was deformed. The results were compared to the original volumes. The size of the volumes was about $128 \times 128 \times 100$ voxels with a voxel size 3.9 mm. The matching error is defined as the shortest Euclidean distance from each model node to the surface in the MR volume.

Ten different prior models were tested. The model that produced the smallest average error was selected out of 20 patients. The results are shown in Table 1a. The error corresponds to about 5 mm. If linear interpolation was used instead of shape based interpolation, the error would be about 5% higher. Fig. 6 shows the deformed model superimposed onto the segmented MR volume in the best case (patient 20, $T=1.03$, $LL=0.93$, $LR=0.90$ voxels) and in the worst case (patient 15, $T=1.25$, $LL=1.8$, $LR=1.21$ voxels). The overall match is good, except for the left lung in Fig. 6b. In general, the highest matching error is concentrated on the areas where the distance to the nearest back-projected vector is

high. The time to create the deformed model from the contours is less than one second with a Sun Ultra10 workstation.

Two simple matching methods were used for comparison: 1) The centers of mass of the contours were matched, 2) The contours were affine registered. The results using these simple matching methods and the elastic deformation method presented in this paper are represented in Table 1b. The column 'Mean' is the mean error for the thorax and lungs of all 20 patients (20 patients and 3 objects leading to 60 measures). The columns 'Min' and 'Max' represent the lowest and the highest value out of 60 matching errors.

Object	Error	Stdev	Max	Method	Mean	Min	Max
T	1.22	0.91	5.4	Mass	2.81	1.47	6.60
LL	1.19	0.91	4.8	Affine	1.61	0.96	3.01
LR	1.21	0.90	4.6	Elastic	1.21	0.85	1.80

Table 1. a) Mean error ($N=20$), standard deviation and maximum error (in voxels) for thorax (T), left lung (LL) and right lung (LR). b) Mean, minimum and maximum matching errors of 20 patients using different matching methods.

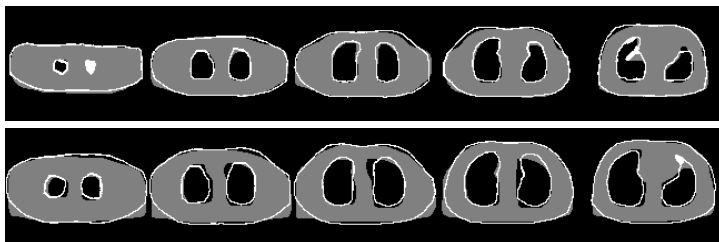


Fig. 6. A deformed model superimposed onto MR images in the best case (top) and in the worst case (bottom).

The effect of the error in imaging geometry was tested. An error of 3 cm in the position of the X-ray source increased the matching error maximally by 10%.

4.3 Extraction of 3D Volume

The same simulation data set was used as in the previous section to define the volume of lungs from projections. The model producing the lowest error was chosen. The average error for right and left lungs were 5% and 7%, respectively. The maximum error was 14% and the minimum error less than 1%.

4.4 Thorax Library

A method was developed and tested to choose the best model from the prior model library to be used with each separate patient. The idea was to test if the

shape of 2D contours in X-ray images has a relation to the 3D shape of the areas far from the back-projected vectors. For example, if a model library contains two models, a cube and a ball, and the 2D contours are circles, the ball-shaped model should be chosen better.

Altogether 90 parameters were calculated from the contours in both directions. These parameters include harmonic coefficients up to the 10th order, different moments, lengths and the area of the object. The differences between the parameters of each model and patient data were calculated. Moreover, several other parameters were defined, such as an error after affine registration. Each model was matched with a data set of 15 different patients and the error was calculated. Thereafter, a linear regression analysis was applied to find out the best linear model to calculate the matching error between a model and a patient using the parameters defined from X-ray images. The best prior model for a patient is the one which gives the lowest matching error using the linear model. The goodness of the model was tested with the data set of 15 patients, and also with a set of 5 patients who were not included in the regression analysis.

If the model giving the lowest error was correctly chosen, the average error in 3D surface reconstruction for thorax, left lung and right lung would be 1.10 voxels. The corresponding value for the model producing the lowest average error was 1.21, as reported above. This means that the error would be about 10% lower in the optimal case. When the linear model was applied, the results for a data set used to create the model was about 2% lower and for the whole data set 1% higher than with the lowest average error model. Thereby, the statistical model is not able to choose the best model from the library with given contours.

5 Discussion

A method was proposed to deform a 3D geometric prior model based on X-ray projections of a patient. The 3D model generated does not describe the anatomy of the patient as well as a model extracted, for example, from MR images, but is a good trade off between accuracy and cost. The accuracy of the elastic matching is superior to affine registration tested. The absolute value of the error was 1.21 voxels using $128 \times 128 \times 100$ volumes. So far, it is not known what is the correlation between the geometric error of the model and the accuracy of MCG/ECG source localization.

The segmentation method developed is robust and fast. Moreover, the construction of the prior model is easy because only one X-ray image with segmented contours is needed. So far, we have applied the method to thorax images. However, to validate the method, it should also be tested with other types of X-ray images.

The pose, the size and the orientation of the prior model should approximately correspond to the patient data. Otherwise, the model has to be coarsely registered with the patient data. If the variability of the shape in the patient data is large, the coarse registration does not solve the problem. Therefore, we used a thorax library to select the best model. However, the shape parameters of the 2D contours did not contain enough information to choose the best model

from the library. The analysis should be continued by using intensity information of X-ray images with the shape parameters. Another approach would be to use a statistical mean model and to deform it using statistically defined deformation modes. After deformation the model should follow the positions defined by the back-projected vectors.

The accuracy of the 3D reconstruction method could be improved by using more than two X-ray projections. However, the improvement of the geometric accuracy compared to the extra dose captured by a patient should be validated. Moreover, a calibration system to produce X-ray images in specific angles should be used.

Besides of the described applications, the method can be used to create patient specific 3D heart models from fluoroscopic images. These models can be fused to the body surface potential mapping system used in a catheterization laboratory. The method could be also applied in registration of 3D images with 2D projections or as an initialization in model based segmentation.

Acknowledgements

The authors express thanks to The Department of Radiology, Helsinki University Central Hospital, Finland and Oy IMIX Ab, Tampere, Finland for providing MR volumes and X-ray images for the study

References

1. J. Nenonen. Solving the inverse problem in magnetocardiography. *IEEE Eng. Med. Biol.*, 13:487–496,1994. 192
2. D. Terzopoulos, A. Witkin and M. Kass. Constraints on Deformable Models: Recovering 3D Shape and Nonrigid Motion. *Artificial Intelligence*, 36:91–123,1988. 192
3. E. Bardinet, L. Cohen and N. Ayache. A Parametric Deformable Model to Fit Unstructured 3D Data. *CVGIP: Image Understanding*, 71(1):39–54,1998. 192
4. T. Sederberg and S. Parry. Free-form deformation of solid geometrical models. *SIGGRAPH*, 20:151–160,1986. 192
5. H. Hoppe, T. DeRose, T. Duchamp, J. McDonald and W. Stuetzle. Surface Reconstruction from Unorganized Points. *Computer Graphics*, 26(2):71–78,1992. 193
6. R. Poli, G. Coppini and G. Valli. Recovery of 3D Closed Surface from Sparse Data. *CVGIP: Image Understanding*, 60(1):1–25,1994. 193
7. A. Laurentini. How Far 3D Shapes Can Be Understood from 2D Silhouettes. *IEEE PAMI*, 17(2):188–195,1995. 193
8. J. Lötjönen, P-J. Reissman, I. E. Magnin and T. Katila. Model Extraction from Magnetic Resonance Volume Data Using the Deformable Pyramid. *Medical Image Analysis*, 1999, in press. 193, 194
9. J. Canny. A computational approach to edge detection. *IEEE Trans. PAMI*, 8:679–698,1986. 193
10. T. F. Cootes, C. J. Taylor, D. H. Cooper and J. Graham. Active shapes models—their training and application. *Computer Vision and Image Understanding*, 61(1):38–58,1995. 195

11. G. Székely, G. Kelemen, C. Brechbühler and G. Gerig. Segmentation of 2-D and 3-D objects from MRI volume data using constrained elastic deformations of flexible Fourier contour and surface models. *Medical Image Analysis*, 1:19–34,1996. 195
12. J. Lötjönen, P-J. Reissman, I. E. Magnin, J. Nenonen, and T. Katila. A Triangulation Method of an Arbitrary Point Set for Biomagnetic Problems. *IEEE Trans. Magn.*, 34(4):2228–2233,1998. 195, 197